

Unsteady surfactant-laden liquid plug propagation: A model for surfactant replacement therapy

Ufuk Olgac and Metin Muradoglu

Koc University, Department of Mechanical Engineering,
Rumeli Feneri Yolu, Sariyer, 34450, Istanbul, Turkey
uolgac@ku.edu.tr, mmuradoglu@ku.edu.tr

Abstract

Pulmonary surfactant is essential in reducing the surface tension on the liquid film that coats the inner surface of the airways. Surfactant-deficiency may result in respiratory distress syndrome (RDS), which is especially common in prematurely born neonates. Surfactant replacement therapy (SRT) is a standard treatment, in which a liquid plug with exogenous surfactant is instilled in the trachea, which subsequently propagates by inspiration and spreads the exogenous surfactant to the airways. The efficacy of the treatment depends on various parameters such as the size of the liquid plug, inspiration frequency and the physical properties of the exogenous surfactant. We performed unsteady simulations of surfactant-laden liquid plug propagation using finite-difference/front-tracking method in order to comprehend and improve the dynamics of the treatment.

Keywords: Liquid plug, surfactant transport, surfactant replacement therapy, front-tracking.

Introduction

Prematurely born neonates may develop respiratory distress syndrome (RDS), as their lungs are not mature enough to produce sufficient amounts of surfactants. Surfactants reduce the surface tension on the thin layer of liquid that coats the inner surface of the airways and the alveoli; and therefore, reduce the work required to expand the lungs with each breath. Surfactant replacement therapy (SRT) is a standard treatment for premature neonates suffering from RDS [1, 2]. In SRT, liquid with exogenous surfactant is instilled in the trachea and form a liquid plug, which subsequently propagates through the trachea by inspiration and spreads the exogenous surfactant to the airways. Liquid may be instilled into the pulmonary airways in other medical treatments such as partial liquid ventilation (PLV) [3, 4] and drug delivery [5, 6].

Liquid plugs may as well be formed internally in the airways. The inner surface of the airways is covered with a thin layer of liquid and this layer may become unstable and form a plaque due to capillary instabilities [7]. In case of surfactant deficiency, the surface tension forces acting on the liquid film increases and liquid plug formation becomes more probable.

Externally induced or internally formed, liquid plugs propagate in the airways due to airflow. The durability of the liquid plugs depends on the leading and trailing film thicknesses. If the leading film thickness is smaller (greater) than the trailing film thickness, the liquid plug

losses (gains) mass and the liquid plug becomes smaller (bigger) and eventually ruptures. In SRT, the liquid plug contains exogenous surfactant and the airways are surfactant-deficient. As the liquid plug is propagating, surfactant is absorbed onto the trailing film and thickens it. In other words, the liquid plug wets the walls of the airway as it is passing through and it eventually ruptures and disappears. The ultimate goal of the therapy is to carry surfactant not only to the upper airways, but also to the lower airways and the alveoli. The motivation behind this study is to investigate the conditions for the most effective delivery of surfactant into the airways and hence improve the efficacy of the treatment.

Another important aspect in SRT is the mechanical stresses that act upon the epithelial cells. Pulmonary epithelial cells might get damaged due to the mechanical stresses that occur when the liquid plug is moving over them [8]. Surfactants have been shown to decrease the magnitude of the stresses, reducing the damage on the epithelial cells [8]. Another motivation of this study is hence to investigate the mechanisms of how surfactants might reduce the damage on the epithelial cells.

It was shown both experimentally [9] and analytically [10] that if the plug is long enough to neglect the interactions between the leading and trailing menisci, the trailing film thickness is the same as the film thickness that would be deposited by a semi-infinite bubble. For semi-infinite bubbles, the trailing film thickness is given by Taylor's law [11] and is dependent

$\beta_s = RT\Gamma_\infty/\sigma_s$ is the elasticity number (R is the ideal gas constant and T is the absolute temperature). The physicochemical parameter β_s is a measure of the sensitivity of interfacial tension to variations in surfactant concentration. In the high interfacial surfactant concentration limit ($\Gamma \sim \Gamma_\infty$), Eq. (7) results in unphysical negative surface tension values. To avoid this, Eq. (7) is slightly modified as

$$\sigma = \sigma_s \left[\max(\varepsilon_\sigma, 1 + \beta_s \ln(1 - \frac{\Gamma}{\Gamma_\infty})) \right], \quad (8)$$

where ε_σ is taken as 0.05 in the present study. The surfactant concentration Γ evolves by [18]

$$\frac{\partial \Gamma}{\partial t} + \nabla_s \cdot (\Gamma \vec{u}_s) = D_s \nabla_s^2 \Gamma + \dot{S}_\Gamma \quad (9)$$

where the gradient operator along the interface is defined as

$$\nabla_s = \nabla - \vec{n}(\vec{n} \cdot \nabla). \quad (10)$$

In Eq. (9), \vec{u}_s is the tangential velocity on the interface, D_s is the diffusion coefficient along the interface and \dot{S}_Γ is the source term given by

$$\dot{S}_\Gamma = k_a C_s (\Gamma_\infty - \Gamma) - k_b \Gamma, \quad (11)$$

where k_a and k_b are adsorption and desorption coefficients, respectively and C_s is the surfactant concentration in fluid immediately adjacent to the interface. The bulk surfactant concentration C is governed by the advection-diffusion equation in the form

$$\frac{\partial C}{\partial t} + \nabla \cdot (C \vec{u}) = \nabla \cdot (D_{co} \nabla C), \quad (12)$$

where the coefficient D_{co} is related to the molecular diffusion coefficient D_c and the indicator function I as

$$D_{co} = D_c (1 - I(r, z, t)). \quad (13)$$

The source term is related to the bulk concentration by [19]

$$\dot{S}_\Gamma = -D_{co} (\vec{n} \cdot \nabla C|_{\text{interface}}). \quad (14)$$

The boundary condition at the interface given by Eq. (14) is first converted into a source term in a conservative manner by assuming that all the mass transfer between the interface and the bulk takes place in a thin adsorption layer adjacent to the interface. In this method, total amount of mass adsorbed on the interface is distributed over the adsorption layer and added to the bulk concentration evolution equation as a negative source term in a conservative manner. Equation (12) thus becomes

$$\frac{\partial C}{\partial t} + \nabla \cdot (C \vec{u}) = \nabla \cdot (D_{co} \nabla C) + \dot{S}_C \quad (15)$$

where \dot{S}_C is the source term evaluated at the interface and distributed onto the adsorption layer in a conservative manner. With this formulation, all the mass of the bulk surfactant to be adsorbed by the interface has been already consumed in the adsorption layer before the interface. Hence, the boundary condition at the interface simplifies to be $\vec{n} \cdot \nabla C|_{\text{interface}} = 0$.

The flow equations (Eqs. (1) and (2)) are solved fully coupled with the evolution equations for interfacial concentration, Eq. (9), and for bulk concentration, Eq. (15), by the finite-difference/front-tracking method [15]. The momentum and the continuity equations are discretized by using a first-order time integration method and a second-order centered difference approximation for the spatial derivatives. The discretized equations are solved on a stationary, staggered Eulerian grid by using the marker-and-cell method [20]. The bulk surfactant concentration is stored at the same location as the pressure on the staggered grid. The evolution equation for the bulk surfactant concentration is solved fully coupled with the flow equations by using second-order centered differences for the spatial derivatives and a first-order Euler method for the time integration. No-slip and no-flux boundary conditions are applied at the tube wall, while the symmetry is used at the tube centerline.

A separate Lagrangian grid is used to track the liquid-gas interface. The Lagrangian grid consists of linked marker points (the front) that move with the local flow velocity interpolated from the stationary Eulerian grid. The piece of the Lagrangian grid between two marker points is called a front element. The interfacial surfactant concentration equation, Eq. (9), is solved on the Lagrangian grid by using second-order centered differences for the spatial derivatives and a first-order Euler method for the time integration. The Lagrangian grid is also used to find the surface tension, which is then distributed onto Eulerian grid points near the interface by using Peskin's cosine distribution function [21], and added to the momentum equations as body forces as described by Tryggvason et al. [22].

At each time step, the indicator function is computed and is used to set the fluid properties in the liquid and gas phases. To do this, unit magnitude jumps are distributed in a conservative manner on the Eulerian grid points near the interface by using Peskin's cosine distribution function [21] and are then integrated to compute the indicator function everywhere. The computation of the indicator function requires solution of a separable Poisson equation and yields a smooth transition of the indicator function across the interface. Then, the fluid properties are set as a function of the indicator function. The indicator function is also used to distribute the surfactant source term in the adsorption layer as described in [15].

The Lagrangian grid is restructured at every time step by deleting the front elements that are smaller than a prespecified lower limit and by splitting the front elements that are larger than a prespecified upper limit in the same way as described by Tryggvason et al. [22] to keep the front element size nearly uniform and comparable to the Eulerian grid size. Restructuring the Lagrangian grid is crucial since it avoids unresolved wiggles due to small elements and lack of resolution due to large elements. Note that restructuring the Lagrangian grid is performed such that the mass conservation is strictly satisfied for the surfactant at the interface. The details of the front-tracking method can be found in the works of Unverdi and Tryggvason [16] and Tryggvason et al. [22]. Readers are referred to Muradoglu and Tryggvason [15] for a complete description of the treatment of the soluble surfactant within the framework of finite-difference/front-tracking method.

Problem statement

We have used the Weibel model as a representation of the human lung [23]. In this model, human lung is assumed to be a symmetric, dichotomous branching tree, in which the mean length of an airway is proportional to its diameter and for which the airway volume for each generation is constant. Taking trachea as the zeroth generation, the number of airways at generation n is $N = 2^n$ and the mean airway diameter is $d_n = d_o 2^{-n/3}$, where d_o is the diameter of the trachea ($0 \leq n \leq 18$). Following Cassidy et al. [9], we assume that a neonatal lung may be modeled to an adult lung starting at generation 7 and the rest of the generations $7 \leq n \leq 18$. Typical neonatal tracheal diameter and tidal volume (TV) is 0.3 cm and 6 ml, respectively [24]. Assuming an inspiration time of 0.7 s for an infant, the tracheal velocity could be calculated from the tidal volume divided by the inspiration time and cross-sectional area to be 121 cm/s. In Table 1, the diameter, number of airways, tidal volume, mean flow velocity U , Capillary number (Ca) and Reynolds number ($Re = \rho U r_n / \mu$) are given in generations $0 \leq n \leq 11$ of a neonatal lung. For a neonatal, Re and Ca numbers are in the range of $0.25 \leq Re \leq 40$ and $0.008 \leq Ca \leq 0.1$ for generations $0 \leq n \leq 11$. We have chosen generation 0,3,6 and 9 as representatives of various flow regimes in an infant's lung and performed our simulations in these generations.

We based our calculations on a commonly used surfactant in SRT, Survanta, for which the density is $\rho = 940 \text{ kg/m}^3$, viscosity is $\mu = 0.042 \text{ Pa}\cdot\text{s}$, and surface tension is $\sigma = 0.025 \text{ N/m}$ [9]. This value of surface tension is assumed to form on the interface only when the interfacial surfactant concentration is close to the maximum packing concentration, Γ_∞ . This is ensured when the clean interfacial surface tension in Eq.

Table 1: Various parameters in a neonatal lung at generations 0-11

N	d (cm)	N	TV (ml)	U (cm/s)	Re	Ca
0	0.300	1	6.000	121.3	40.71	0.102
1	0.238	2	3.000	96.2	25.65	0.081
2	0.189	4	1.500	76.4	16.16	0.064
3	0.150	8	0.750	60.6	10.18	0.051
4	0.119	16	0.375	48.1	6.41	0.040
5	0.094	32	0.188	38.2	4.04	0.032
6	0.075	64	0.094	30.3	2.54	0.025
7	0.060	128	0.047	24.1	1.60	0.020
8	0.047	256	0.023	19.1	1.01	0.016
9	0.038	512	0.012	15.2	0.64	0.013
10	0.030	1024	0.006	12.0	0.40	0.010
11	0.024	2048	0.003	9.5	0.25	0.008

(8) is taken as $\sigma_s = 0.5 \text{ N/m}$. The change in surface tension with respect to interfacial surfactant coverage is shown in Fig. 2.

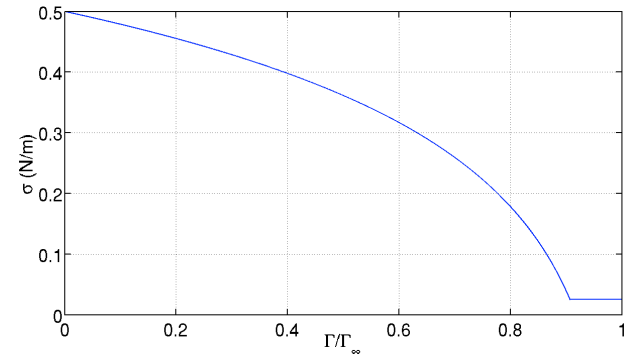


Fig.2 Variation of surface tension with respect to interfacial surfactant coverage.

We consider a long straight channel, which represents an airway; of length L and radius R as sketched in Fig. 1. Fully developed velocity profile is specified at the inlet with an average velocity of U (see Table 1 for values of U at various generations) given as

$$U = \frac{\pi r_{\text{int}}^2 \bar{u}_g + \pi (R^2 - r_{\text{int}}^2) \bar{u}_l}{\pi R^2} \quad (16)$$

where r_{int} is the radius of the interface, and, \bar{u}_g and \bar{u}_l are the average velocities in the gas and liquid phases, respectively, whose ratio is given as

$$\frac{\bar{u}_g}{\bar{u}_l} = \frac{(r_{\text{int}}/R)^2 \mu_l}{1 - (r_{\text{int}}/R)^2 \mu_g} + 2. \quad (17)$$

The velocity profiles in the gas and the liquid phases at the inlet are then given as

$$u_l = 2\bar{u}_l \frac{1 - (r/R)^2}{1 - (r_{\text{int}}/R)^2}, \quad (18)$$

$$u_g = 2\bar{u}_l + 2(\bar{u}_g - 2\bar{u}_l)(1 - (r/r_{\text{int}})^2).$$

Pressure is set to zero at the outlet and no-slip boundary conditions are applied at the wall. The non-dimensional plug length is defined as $L_p^* = L_p/R$, where L_p is defined as the distance between the trailing and the leading menisci on the channel axis. Computations are performed for $L_p^* = 0.5 - 4$. An initial surfactant-free run is performed for each L_p^* at each generation in order to determine the trailing film thickness. Thereafter, using the pre-determined trailing film thickness as an initial condition for the trailing and leading film thicknesses, surfactant-free computations are performed. In surfactant-laden cases, surfactant is added to the system with a concentration of 25 mg/ml, which is the standard for Survanta in SRT [25]. Surfactant is instilled in the liquid plug and on the trailing film as shown in Fig. 1.

The governing non-dimensional parameters are given as follows

$$\begin{aligned} \text{Re} &= \frac{\rho_l U L}{\mu_l}; & \text{Ca} &= \frac{\mu_l U}{\sigma_s}; & \text{Pe}_c &= \frac{U L}{D_c}; \\ \text{Pe}_s &= \frac{U L}{D_s}; & k &= \frac{k_a C_\infty}{k_b}; & \text{Bi} &= \frac{k_b L}{U}; \\ \text{Da} &= \frac{\Gamma_\infty}{L C_\infty}; & \beta_s &= \frac{R T \Gamma_\infty}{\sigma_s}, \end{aligned} \quad (19)$$

where Re , Ca , Pe_c , Pe_s , k , Bi , Da , and β_s are the Reynolds number, the capillary number, the Peclet number based on bulk surfactant diffusivity, the Peclet number based on interfacial surfactant diffusivity, the dimensionless adsorption depth, the Biot number, the Damkohler number and the elasticity number, respectively. Re and Ca numbers are given in Table 1 for the generations considered. Pe_c and Pe_s are taken as 100 and 1000, respectively, following Fujioka and Grotberg [13]. Non-dimensional adsorption depth is calculated to be $k = 2500$ with $k_a = 1.7 \text{ m}^3/\text{kg s}$ and $k_b = 1.7 \times 10^{-2} \text{ s}^{-1}$, adsorption and desorption coefficients for pulmonary surfactant [26, 27]. Biot and Damkohler numbers are calculated to be $\text{Bi} = 2.1 \times 10^{-5}$ and $\text{Da} = 8.3 \times 10^{-5}$, respectively, with the packing interfacial concentration $\Gamma_\infty = 3.1 \times 10^{-6} \text{ kg/m}^3$ [28]. Elasticity number is taken as 0.4.

Results and discussion

We have performed simulations at various generations with various non-dimensional plug lengths. For the surfactant-free cases, as demonstrated in Fig. 3, in the upper airways (higher Ca numbers), the trailing film thickness varies with plug length for $L_p^* < 2.0$, which means that for plugs with plug size larger than the channel width, the trailing film thickness is the same as would be for a semi-infinite bubble as also observed by Fujioka and Grotberg [12]. For the lower airways (lower Ca numbers), trailing film thickness does not change with L_p^* . It is also observed in Fig. 3 that the discrepancy between the analytical solution for film thickness for a semi-infinite bubble given by Taylor's Law [11] and the computed film thicknesses decreases as we go from the upper to the lower airways. The relative error between theory and the computed film thicknesses are 12.2 %, 5.2 %, 3.6 % and 6.2 % for generations 0, 3, 6 and 9, respectively. The analytical solution depends on the capillary number based on plug speed and is given as

$$\frac{h_\infty}{R} = \frac{1.34 \text{Ca}^{2/3}}{1 + 1.34 \times 2.5 \text{Ca}^{2/3}}. \quad (19)$$

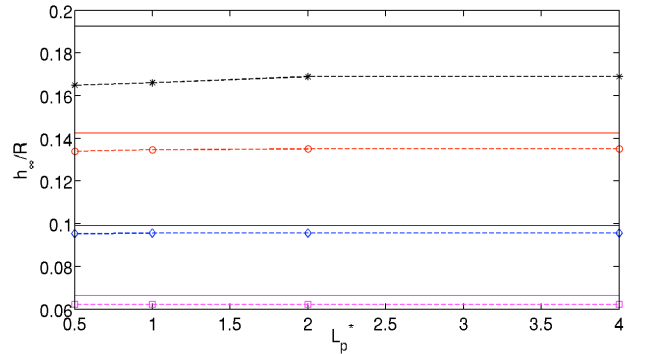


Fig.3 Trailing film thickness for the surfactant-free cases at various generations with respect to non-dimensional plug length. Black, red, blue and magenta represent generation 0,3,6 and 9 respectively. Symbols with dash lines represent the calculated values and solid lines represent film thickness values calculated from Taylor's law [11].

A comparison of trailing film thickness for surfactant-free and surfactant-laden cases for various generations is presented in Fig. 4. It is observed in Fig. 4 that surfactant thickens the trailing film and decreases the size of the liquid plug. At all generations, the trailing film thickness in the surfactant-laden case is greater than in the surfactant-free case. As we go from the upper airways to the lower airways, the capillary number decreases, which leads to decreased trailing film thickness, as well as decreased relative plug speed. This is the reason why plug in the highest generation, i.e. generation 0, is the one that propagated most. In most of the surfactant-free cases the trailing film thickness is almost flat everywhere, except generation 0. In generation 0, we observe a wake in the

trailing film thickness whose propagation speed is much less than the speed of the plug. We ascribe the formation of this wake to the high Reynolds number (dominant inertial forces) in this generation, i.e. $Re=40$. In all the surfactant-laden cases, we observe an initial thinning close to the beginning of the airway, followed by a small wake formation. The reason for this is the non-uniform interfacial surfactant distribution on the trailing film, which results in formation of Marangoni stresses. This non-uniform interfacial surfactant distribution is shown both in Fig. 5 and 6. As shown in Fig. 5, the wake is formed in the low interfacial surfactant concentration (high surface tension) region, since the liquid is pulled into this region due to the Marangoni stresses in all generations. We also observe in Fig. 6 that the gradient in interfacial surfactant concentration is sharper in higher generations, which leads to an increase in Marangoni stresses and a more pronounced wake formation. Another important observation in Fig. 5 and 6 is that the interfacial surfactant is spread more uniformly on the trailing film at lower generations. We believe this is because of the smaller (higher) trailing film thickness in lower (higher) generations: Most of the bulk surfactant in the liquid plug is stuck in the distal trailing film for the upper airways, whereas in the lower airways, due to the decreased thickness of the trailing film, the bulk surfactant is carried more distal with the plug and is more uniformly spread in the trailing film. We demonstrate this phenomenon in Fig. 7 in more detail, where the initial evolutions of interfacial and bulk surfactant concentrations are presented for generation 3. It is observed that some part of the surfactant in the liquid plug is trapped in the trailing liquid film whereas the remaining part is accumulated at the leading meniscus of the plug.

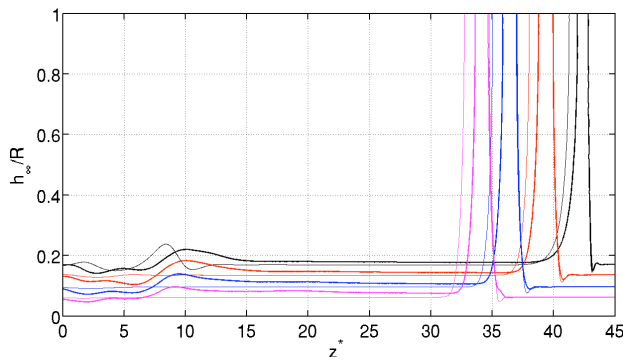


Fig.4 Trailing film thickness at various generations at $t^* = 27$. Black, red, blue and magenta represent generation 0,3,6 and 9 respectively; thick and thin lines represent surfactant-free and surfactant-laden cases, respectively.

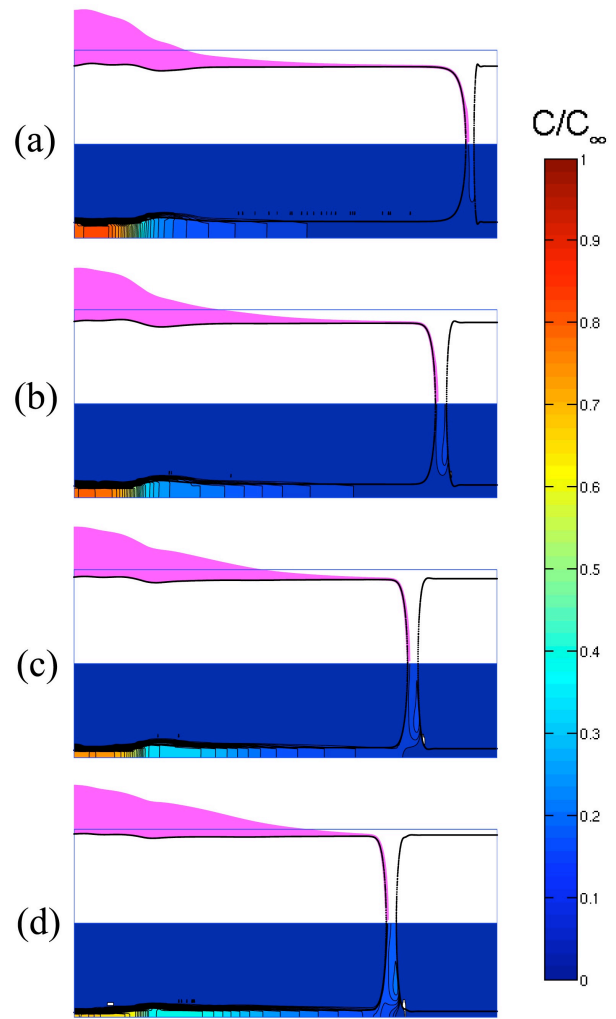


Fig.5 Interfacial surfactant concentration (upper side) and bulk surfactant concentration (lower side) at $t^* = 27$ for generations (a) 0, (b) 3, (c) 6 and (d) 9. The axis are not-to-scale.

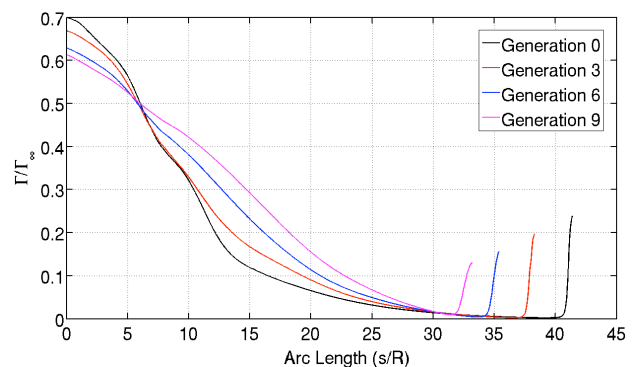


Fig.6 Interfacial surfactant concentration on the trailing film and trailing meniscus at $t^* = 27$ for various generations.

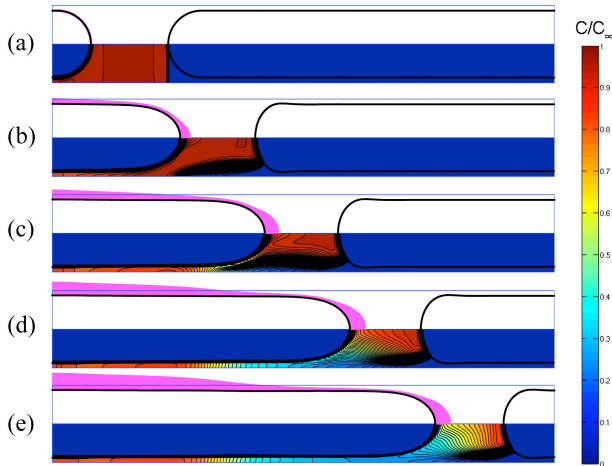


Fig.7 Interfacial surfactant concentration (upper side) and bulk surfactant concentration (lower side) at (a) $t^* = 0$, (b) $t^* = 0.8$, (c) $t^* = 1.6$, (d) $t^* = 2.4$ and (e) $t^* = 3.2$ for generation 3.

In all the surfactant-free cases, the variation of plug length is below 1.0% (approximately steady-state). The change in plug length in the surfactant-laden cases for various generations at various initial plug sizes is presented in Fig. 8. The initial drop in the length of the plug at generation 0 is mainly due to the high Re number in this generation, which leads to a wake formation in the surfactant-free cases. An important observation is that when the initial plug length is small, the plug becomes smaller more rapidly in the lower airways compared to the upper airways. We could conclude that the initially small plugs have an increased tendency to rupture in the lower airways.

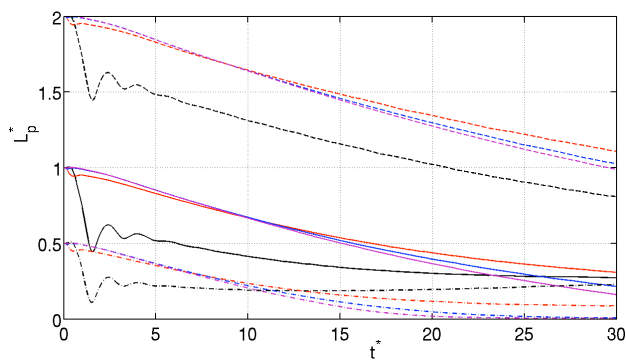


Fig.8 Change in non-dimensional plug length in time. Black, red, blue and magenta represent generation 0,3,6 and 9 respectively. Initial non-dimensional plug length is 0.5, 1.0, 2.0, for dash-dot, solid and dashed lines, respectively.

We have performed further computations in order to investigate the effects of the amount of surfactant initially instilled with the liquid plug. For this purpose we have increased the initial surfactant concentration from 25 mg/ml to 50 mg/ml and 100 mg/ml. The Damkohler number accordingly decreased to $Da = 4.1 \times 10^{-5}$

and $Da = 2.1 \times 10^{-5}$, respectively. In order to keep the adsorption-desorption ratio constant, we also changed the non-dimensional adsorption depth to $k = 5000$ and $k = 10000$, respectively. As demonstrated in Fig. 9, increasing the initial bulk surfactant concentration leads to a more rapid decrease in the plug size as the plug propagates in the airways in all generations. Therefore, we could conclude that increasing the amount of surfactant instilled with the liquid plug might lead to an earlier rupture of the plug. When the objective is to deliver the liquid plug to the lower airways, increasing the initial surfactant instilled with the plug may not be advantageous.

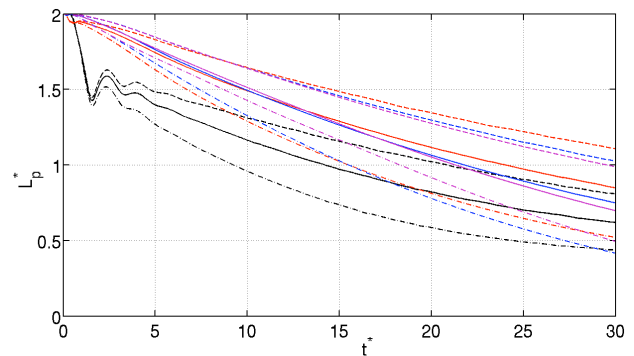


Fig.9 Change in non-dimensional plug length in time for various initial bulk surfactant concentrations. Black, red, blue and magenta represent generation 0,3,6 and 9 respectively. Initial surfactant concentration is 25mg/ml, 50 mg/ml and 100 mg/ml for dashed, solid and dash-dot lines, respectively.

The mechanical stresses that act upon the epithelial cells that cover the inner surface of the airways are an important aspect in SRT. As the plug is propagating, it leads to high shear stresses and abrupt changes in pressure over the region it passes through, which might damage the epithelial cells in this region. In Fig. 10 and 11, non-dimensional pressure and non-dimensional shear stress are presented, respectively, for both the surfactant-free and surfactant-laden cases. The pressure and the shear stress are non-dimensionalized as $P^* = P / (\sigma / R)$ and $\tau^* = \tau / (\sigma / R)$. We observe that in both cases as we go from the upper to the lower airways, the pressure drop along the liquid plug and the shear stresses that occur in the plug region decrease. We also observe that pressure drop along the liquid plug is slightly smaller in the surfactant-laden case compared to the surfactant-free case. This might be because of the slightly increased plug speed in the surfactant-laden case. Looking at the shear stresses, it is observed that the high stresses at the leading meniscus of the plug are decreased for the surfactant-laden cases and that this behavior is more pronounced in the lower airways compared to the upper airways. We could conclude that introduction of surfactants in liquid plug propagation might reduce the potential damage on epithelial cells, especially in the

lower airways. It is also important in SRT that when an instilled plug reaches the lower airways, it still contains some surfactant so that the reduction in epithelial cells is reduced.

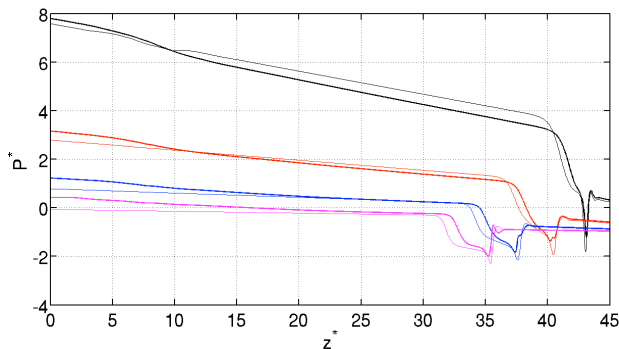


Fig.10 Non-dimensional pressure on the airway wall at various generations at $t^* = 27$. Black, red, blue and magenta represent generation 0,3,6 and 9 respectively; thick and thin lines represent surfactant-free and with surfactant cases, respectively.

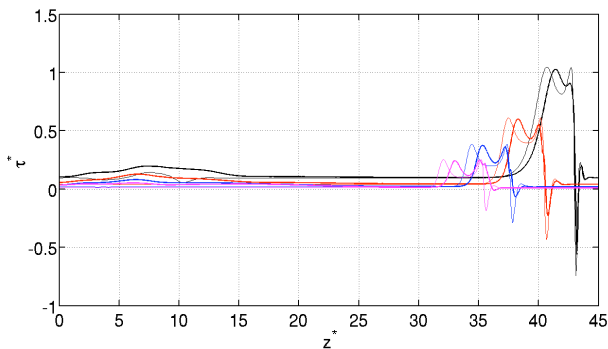


Fig.11 Non-dimensional shear stress on the airway wall at various generations at $t^* = 27$. Black, red, blue and magenta represent generation 0,3,6 and 9 respectively; thick and thin lines represent surfactant-free and with surfactant cases, respectively.

Conclusions

We have performed computations for the surfactant-free and surfactant-laden propagation of a liquid plug in pulmonary airways of a neonatal at various generations using finite-difference/front-tracking method. We found that for the surfactant-free case, when the liquid plug size is larger than the channel width, the trailing film thickness is independent of the liquid plug size and could be predicted by Taylor's law. We have observed that the trailing film thickness increases with the introduction of surfactants in the liquid plug. The interfacial surfactant distribution on the trailing film is more uniform in the lower airways compared to the upper airways. Liquid plugs with comparably smaller sizes tend to rupture more easily in the lower airways compared to the upper airways. We have also observed that increasing the amount of initially instilled surfactant in the liquid plug results in a more rapid rupture of the plug. We could

therefore conclude that instead of increasing the initial surfactant concentration, increasing the plug size might be a better method to increase the efficacy of the treatment. We have also observed that surfactants reduce the shear stresses and potential damage to epithelial cells especially in the vicinity of the leading meniscus of the plug.

Acknowledgements

The first author (UO) is supported by the Scientific and Technological Research Council of Turkey (TUBITAK) through BIDEB.

References

- [1] A. Corbet, R. Bucciarelli, S. Goldman, M. Mammel, D. Wold, W. Long, Decreased Mortality-Rate among Small Premature-Infants Treated at Birth with a Single Dose of Synthetic Surfactant - a Multicenter Controlled Trial, *J Pediatr*, 118 (1991) 277-284.
- [2] A.H. Jobe, Drug-Therapy - Pulmonary Surfactant Therapy, *New Engl J Med*, 328 (1993) 861-868.
- [3] R.B. Hirschl, R. Tooley, A.C. Parent, K. Johnson, R.H. Bartlett, Improvement of Gas-Exchange, Pulmonary-Function, and Lung Injury with Partial Liquid Ventilation - a Study Model in a Setting of Severe Respiratory-Failure, *Chest*, 108 (1995) 500-508.
- [4] T.H. Shaffer, M.R. Wolfson, Liquid ventilation: An alternative ventilation strategy for management of neonatal respiratory distress, *Eur J Pediatr*, 155 (1996) S30-S34.
- [5] J.W. Yu, Y.W. Chien, Pulmonary drug delivery: Physiologic and mechanistic aspects, *Crit Rev Ther Drug*, 14 (1997) 395-453.
- [6] Y.L. Zhang, O.K. Matar, R.V. Craster, A theoretical study of chemical delivery within the lung using exogenous surfactant, *Med Eng Phys*, 25 (2003) 115-132.
- [7] R.D. Kamm, R.C. Schroter, Is Airway-Closure Caused by a Liquid-Film Instability, *Resp Physiol*, 75 (1989) 141-156.
- [8] A.M. Bilek, K.C. Dee, D.P. Gaver, Mechanisms of surface-tension-induced epithelial cell damage in a model of pulmonary airway reopening, *J Appl Physiol*, 94 (2003) 770-783.
- [9] K.J. Cassidy, N. Gavriely, J.B. Grotberg, Liquid plug flow in straight and bifurcating tubes, *J Biomech Eng-T Asme*, 123 (2001) 580-589.
- [10] P.D. Howell, S.L. Waters, J.B. Grotberg, The propagation of a liquid bolus along a liquid-lined flexible tube, *J Fluid Mech*, 406 (2000) 309-335.
- [11] P. Aussillous, D. Quere, Quick deposition of a fluid on the wall of a tube, *Phys Fluids*, 12 (2000) 2367-2371.
- [12] H. Fujioka, J.B. Grotberg, Steady Propagation of a Liquid Plug in a Two-Dimensional Channel, *Journal of Biomechanical Engineering*, 126 (2004) 567-577.

- [13] H. Fujioka, J.B. Grotberg, The steady propagation of a surfactant-laden liquid plug in a two-dimensional channel, *Phys Fluids*, 17 (2005) -.
- [14] H. Fujioka, S. Takayama, J.B. Grotberg, Unsteady propagation of a liquid plug in a liquid-lined straight tube, *Phys Fluids*, 20 (2008) -.
- [15] M. Muradoglu, G. Tryggvason, A front-tracking method for computation of interfacial flows with soluble surfactants, *J Comput Phys*, 227 (2008) 2238-2262.
- [16] S.O. Unverdi, G. Tryggvason, A Front-Tracking Method for Viscous, Incompressible, Multi-Fluid Flows, *J Comput Phys*, 100 (1992) 25-37.
- [17] V.G. Levich, *Physicochemical Hydrodynamics*, in, Englewood Cliffs, EUA : Prentice-Hall, 1962.
- [18] H.A. Stone, A Simple Derivation of the Time-Dependent Convective-Diffusion Equation for Surfactant Transport Along a Deforming Interface, *Phys Fluids a-Fluid*, 2 (1990) 111-112.
- [19] C.D. Eggleton, K.J. Stebe, An adsorption-desorption-controlled surfactant on a deforming droplet, *J Colloid Interf Sci*, 208 (1998) 68-80.
- [20] F. Harlow, E. Welch, Numerical Calculation of Time-Dependent Viscous Incompressible Flow of Fluid with Free Surface, *Phys Fluids*, 8 (1965) 2182-2189.
- [21] C.S. Peskin, Numerical analysis of blood flow in heart, *J Comput Phys*, 25 (1977).
- [22] G. Tryggvason, B. Bunner, A. Esmaeeli, D. Juric, N. Al-Rawahi, W. Tauber, J. Han, S. Nas, Y.J. Jan, A Front-Tracking Method for the Computations of Multiphase Flow, *J Comput Phys*, 169 (2001) 708-759.
- [23] E.R. Weibel, D.M. Gomez, Architecture of the Human Lung, *Science*, 137 (1962) 577-585.
- [24] D. Halpern, O.E. Jensen, J.B. Grotberg, A theoretical study of surfactant and liquid delivery into the lung, *J Appl Physiol*, 85 (1998) 333-352.
- [25] R.L. Bissinger, C.A. Carlson, Surfactant, Newborn and Infant Nursing Reviews, 6 (2006) 87-93.
- [26] M.A. Launoisurpas, T. Ivanova, I. Panaiotov, J.E. Proust, F. Puisieux, G. Georgiev, Behavior of Pure and Mixed Dppc Liposomes Spread or Adsorbed at the Air-Water-Interface, *Colloid Polym Sci*, 270 (1992) 901-911.
- [27] D.R. Otis, E.P. Ingenito, R.D. Kamm, M. Johnson, Dynamic Surface-Tension of Surfactant T_a - Experiments and Theory, *J Appl Physiol*, 77 (1994) 2681-2688.
- [28] S. Schurch, H. Bachofen, J. Goerke, F. Possmayer, A Captive Bubble Method Reproduces the Insitu Behavior of Lung Surfactant Monolayers, *J Appl Physiol*, 67 (1989) 2389-2396.